Oscillation annealing and driver/tire load torque estimation in Electric Power Steering Systems

J. Tordesillas Illán, V. Ciarla, and C. Canudas de Wit

***Abstract*— The paper presents several aspects of modeling, observation and control towards a new generation of Electrical Power Steering(EPS) systems. In particular we design an optimal control to reject oscillations of the steering column, then we device a new observer to estimate the internal state variables of the steering column, the driver applied torque (steering wheel torque), and the load torque (tire/ground contact friction). Finally, we also revisited the LuGre tire dynamic friction model by improving the transient behavior between the sticking phases and the dynamic ones. Simulation of the proposed control and observer are shown at the end of the paper using the improved LuGre-tire friction model.**

***Index Terms*— Electric Power Steering systems (EPSs), LQ control, LuGre friction model, observer.**

I. Introduction

Nowadays, the existing Electric Power Steering systems (EPSs) are developed basing on a general driver profile [1], [2]. Future generation of EPSs should be able to propose a torque assistance which may be adapted for different kinds of driver population: young drivers, aged people, disabled people, etc.

A first important step towards the above goals consists in setting a control framework that includes a realistic model of a steering column accounting for all other torque loads involved in a real driving situation (torsion torque due to force sensors flexibility, applied driver forces, and tire-road contact friction forces). The control framework should also include observers that allow to recover signals which are not sensed and a control law that compensates for the column flexibilities. This is completed with a booster-torque-law (power steering torque) specific to the driver population in question. The general architecture that we propose is shown in Fig. 1. This paper concerns with the block 1 (observer/control), and the block 2 (tire-friction model) of Fig. 1, with the additional contribution that the observer also estimate the driver and load torque. The design of the specific reference model (block 3) for non-standard drivers is under current investigation.

The contributions of this paper are:

a) Optimal output control feedback: Based on the steering column model proposed by [3], [4], we redesign a linear optimal control that seeks to cancel oscillation due to column stiffness. This results in an output optimal feedback with an observer included. In addition to cancel oscillation the control design seeks to preserve the open-loop gain between the applied driver torque and the motion of the steering wheel. In that way the low frequency feelings of the driver will not be affected. The observer in this first version was derived assuming that the exogenous inputs (driver and tire-friction torques) were known.

b) Improved LuGre Tire-friction model: The dynamic LuGre Friction model proposed in [5], [6] is here modified to trade the transition between the stick friction component (that dominated when vehicle is stand still), and the self-alignment torque (produced when vehicle in motion). To have a complete tire-friction model is mandatory to test EPS systems.

c) Driver and load torque estimation: The observer previously designed was extended to the case where the exogenous inputs are unknown. This was done assuming the standard hypothesis for observation under unknown input, namely a slow rate of variations of these inputs. In spite of this hypothesis, our results show that these exogenous torques where correctly estimated with a very good precision and very little phase lag.

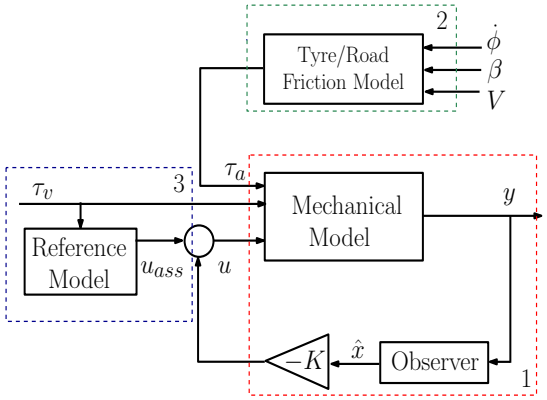

Fig. 1. General architecture of the EPSs: block 1 concerns the observer and the control; block 2 includes the tyre-friction model and block 3 includes the reference model.

The paper is organized following the 3 main items as indicated above.

II. Oscillations annealing

To begin with, it is essential to define the mechanical system that we will take into account. Fig.2 shows an explanatory schema of the system.

C. Canudas-de-Wit and V. Ciarla are with the Laboratoire d'Automatique de Grenoble, UMR CNRS, Grenoble 5528, France (e-mails: carlos.canudas-de-wit@gipsa-lab.inpg.fr, valentina.ciarla@gipsa-lab.grenoble-inp.fr)

TABLE I

CONSTANT PARAMETERS OF THE EPSS

Symbol	Value	Description
J_v	steering wheel inertia	$0.025\ [kg \cdot m^2]$
J_m	motor inertia	$0.00033\ [kg \cdot m^2]$
J_c	steering motor inertia	neglected
J_w	aggregated wheel and rack inertia	neglected
k	steering column stiffness	$100\ [N \cdot m]$
N_1	vehicle steering angle to steering colon ratio	13.67
N_2	motor-steering column gear ratio	17
B_v	damping coeff. associated to the steering wheel	$0.01\ [N \cdot s/m]$
B_m	damping coeff. associated to the motor axis	$0.003\ [N \cdot s/m]$

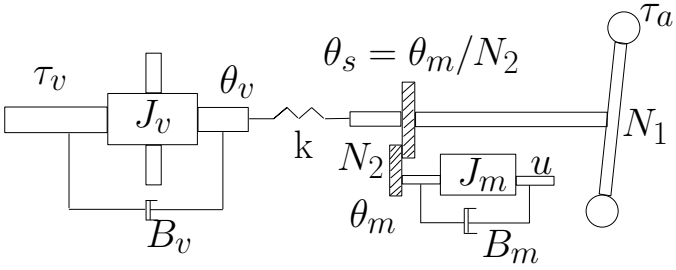

Fig. 2. Mechanical model of the EPSs

A. Column model

The mechanical equations governing the system explained above are (see [3])

$$J_v\ddot{\theta}_v = \tau_v - k(\theta_v - \theta_s) - B_v\dot{\theta}_v \quad (1)$$

$$J_T\ddot{\theta}_s = -k(\theta_s - \theta_v) - N_2^2 B_m\dot{\theta}_s + \frac{\tau_a}{N_1} + N_2 u \quad (2)$$

with $J_T = \left(J_c + N_2^2 J_m + \frac{J_w}{N_1^2}\right)$. The constants of the model are defined in Table I, while θ_v, θ_s and θ_m are, respectively, the steering wheel, the motor-shaft and the motor angles. Both J_c and J_w are neglected for simplicity, but to obtain more precise results it is advisable to introduce these parameters in the calculations. Let

$$x^T = \left(x_1, x_2, x_3\right)^T = \left(\dot{\theta}_v, \dot{\theta}_s, \theta_v - \theta_s\right)^T \quad (3)$$

The model can be formulated into the state-space form

$$\dot{x} = Ax + Bu + Gw$$

with $w = \left(\tau_v, \tau_a\right)^T$ and

$$A = \begin{pmatrix} -\frac{B_v}{J_v} & 0 & -\frac{k}{J_v} \\ 0 & -\frac{N_2^2 B_m}{J_T} & -\frac{k}{J_T} \\ 1 & -1 & 0 \end{pmatrix}; \quad B = \begin{pmatrix} 0 \\ \frac{N_2}{J_T} \\ 0 \end{pmatrix};$$

$$G = \begin{pmatrix} \frac{1}{J_v} & 0 \\ 0 & \frac{1}{N_1 J_T} \\ 0 & 0 \end{pmatrix} = \begin{bmatrix} g_1 & g_2 \end{bmatrix}; \quad (4)$$

It is interesting to observe how the model responds to a variation of the torque exerted by the driver on the steering wheel. To do this, it seems appropriate to compute the transfer function of the steering wheel's angular acceleration $\ddot{\theta}_v$ to the driver's exerted torque τ_v. Such a transfer function is easily computed from the state-space matrices as follows:

$$G_{ol} = \frac{\ddot{\theta}_v}{\tau_v} = T(sI - A)^{-1}G_1$$

where $T = \begin{pmatrix} -\frac{B_v}{J_v} & 0 & -\frac{k}{J_v} \end{pmatrix}$. Fig. 3 shows the frequency response and puts in evidence that the open loop system has a significant peak for a frequency of about 12 Hz that cause substantial oscillations on the steering wheel and that should be avoided so as to improve the driving comfort.

B. Full-state optimal feedback control

To compensate the oscillations an optimal LQR controller is designed. This controller is computed so that the state-feedback law $u = -Kx$ (with K the state-feedback gain) minimizes following cost function:

$$J = \int_0^\infty (x^T Q x + ru^2)\, dt \quad (5)$$

where the constant matrices $Q > 0$ and $r > 0$ are the weighting matrices. For the purpose of annealing the oscillation without impact the low frequency gains of the resulting closed loop, we can select Q such that only the torsion angle and its time derivative is penalized, i.e.

$$J = \int_0^\infty (q_1(x_1 - x_2)^2 + q_2 x_3^2 + ru^2)\, dt$$

Normalizing this cost with $r = 1$, the problem is simplified by selecting Q as

$$Q = \begin{pmatrix} q_1 & -q_1 & 0 \\ -q_1 & q_1 & 0 \\ 0 & 0 & q_2 \end{pmatrix} \quad (6)$$

This results in a cost function with only two parameter to be tuned. The closed-loop transfer function is given by the following equation:

$$G_{cl} = \frac{\ddot{\theta}_v}{\tau_v} = T(sI - (A - BK))^{-1}G_1 \quad (7)$$

with $A - BK$ the closed-loop state space matrix.

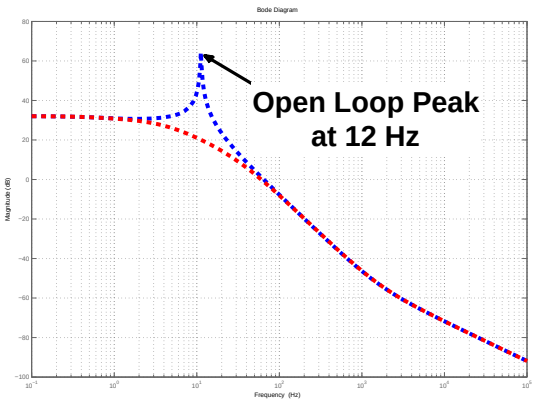

Fig. 3. Open loop (blue) vs closed loop frequency response. Weighting parameters are: $q_1 = 3$ and $q_2 = 12$, $r = 1$.

The benefits of this design can be observed in Fig. 3. The resonance peak that might cause undesirable oscillations have been eliminated thanks to the proposed optimal linear control. Note also that the low-frequency gain has kept unchanged.

C. Optimal "output" feedback controller

All the calculations carried out until now assumed that the whole set of state-space variables was measurable. In commercial products only the motor angle and the torsion torque are measured. This is due to the fact that installation of these additional sensors implies an important extra cost that should be, if possible, avoided.

The previous control problem can be reformulated by assuming only that the motor speed (approximated from motor position sensor) is available. This means that we dispose of the output

$$y = Cx = (0, 1, 0)x = \dot{\theta}_s$$

Assuming as before (this hypothesis will be relaxed latter) that w is measured as well, then the proposed observer has the following form

$$\dot{\hat{x}} = (A - LC)\hat{x} + Bu + Gw + Ly \tag{8}$$

where L is the observer gain to be designed. By the separation principle, the control K is kept as before, and L can be designed either via pole placement method, or via the loop-recovering strategy. In any case, it is suited that the dynamics of the observation error $\dot{\hat{x}} - \dot{x} = \dot{e} = (A - LC)e$ has a fast dynamics and hence a fast convergence of the observer towards the real states.

D. Simulation results

In order to see the performances of the proposed controller, following simulations are carried out using as input to the system the driver's exerted torque profile shown in Fig. 4-a.

1) Open loop behavior: The first simulation concerns the system in open loop. As shown at the Fig. 4-b, once the steering wheel is released by the driver at the time instant $16s$, the steering wheel suffers significant oscillations that would cause an undesirable driving feeling and might even be dangerous when we are in driving situations at fast speeds.

2) Closed-loop behavior under closed-loop: The optimal linear controller computed before has the aim to eliminate the oscillations found in open loop thanks to the assistance motor. As shown at the Fig. 4-c, the oscillations derived from the release of the steering wheel have been satisfactorily compensated by the optimal controller. The behavior of the observer is shown by Fig. 4-d. From this figure we see that the performance of the observer is completely satisfactory.

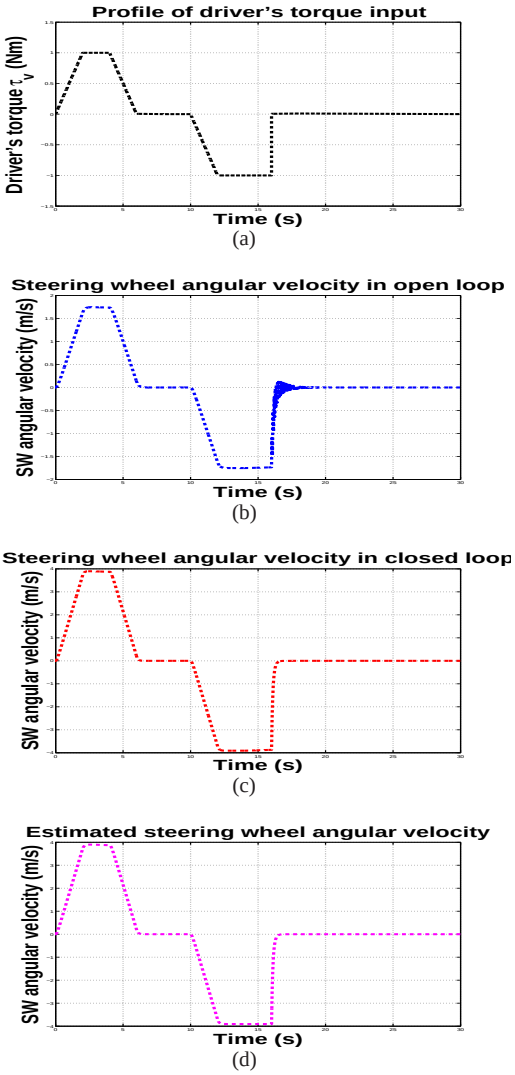

Fig. 4. (a) Real driver's steering torque used for the simulation. (b) Profile of the steering wheel speed in open loop. (c) Profile of the steering wheel speed in closed loop. (d) Estimation of the steering wheel speed.

III. Tire/road contact friction torque

The model used until now takes into account all the elements that go from the steering wheel to the steering shaft. Load torques exerted by tire/road contact need to be consider explicitly in the model. The contact friction force is an important element of the driving it is present in all the different driving situations that a driver may find, and it is the main responsible of the ultimate feeling that the driver will feel during his driving maneuvers.

In general, models for contact forces need to be completed with the mechanical model of the vehicle dynamics as the states/variables between the contact forces and those of the vehicle dynamics are coupled. However to avoid unnecessary complexity (implementing a complete vehicle model it is not essential for the development of our simulations), the model chosen is a simplified model of the tires assuming that the normal force on them is equal to a quarter of the total weight of the vehicle.

Fig. 5 illustrates the longitudinal and the lateral velocity that might appear when driving under the effect of centripetal forces. This lateral force appearing during the turning manoeuvres, is the origin of the slipping, in the direction of the so-called slipping angle β.

So as to prove the validity of the observer, it is implemented in simulation. In the bottom of fig. 4 it can be stated that the performance of the observer is completely satisfactory. To sum up, an observer has been calculated such that the whole state-space has been rebuilt from both the control input and the measurable output. Once all the different states have been estimated, the full state feedback

carried out in section II-B is implemented obtaining very satisfactory results.

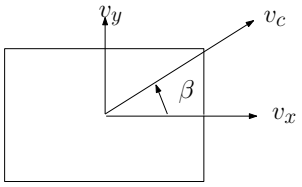

Fig. 5. Forces action on the tire when turning. Slip angle β show the direction of the vehicle resulting velocity

The angle β, is known to depend on the vehicle's speed, v as well as on the radius of curvature, ρ given by the curve traced by the vehicle in a given moment, i.e. $\beta(t) = f(v, \rho)$. The radius of curvature can be considered as being inversely proportional to the steering wheel angle: an infinite radius of curvature means the vehicle is going straight and hence the steering wheel angle is zero. For the reasons advocated before, in our simulations a simple relation between β and the steering wheel angle weighted by the vehicle velocity is considered.

A. Dynamic tyre friction model

We introduce here some modifications to the dynamic LuGre Friction model proposed in [5], [6]. These modifications aim at improving the transition between the sticking friction component (that dominates when vehicle is stand still), and the self-alignment torque (produced when vehicle is in motion). The most important phenomena (components) captured by the model are:

- Sticking torque $M_{sticking}$: it is the torque that opposes the movement of the tyres when turning them around the vertical axis. It is especially important for low speeds of the vehicle.
- Self-alignment torque $M_{self-alig}$: it is the torque that appears as the vehicle speed up, and tends to rotate the wheels around its vertical axis in order to make them return to the straight position.

The dynamic LuGre Friction model proposed in [5], [6] derives from a distributed friction model. It is described by four differential equations, which capture the average behavior of the internal friction states. To introduce this model, let $\bar{z}_i(t)$ $(i = x, y)$, $\hat{z}_y(t)$ denote the internal states of the system:

$$\dot{\bar{z}}_i(t) = v_{ri} - C_{0i}(v_r)\bar{z}_i(t) - \kappa_i^{ss}|\omega r|\bar{z}_i(t) \quad (i = x, y) \tag{9}$$

$$\dot{\hat{z}}_y(t) = \frac{G}{F_n L} v_{ry} - C_{0y}(v_r)\hat{z}_y(t) - - \nu^{ss}|\omega r|\hat{z}_y(t) + \frac{|\omega r|}{L}\bar{z}_y(t) \tag{10}$$

where $v_r = [\ v_{rx} \quad v_{ry}\ ]^T$ is the vector of the relative speeds:

$$v_{rx} = \omega r - v cos(\beta) \tag{11}$$

$$v_{ry} = -v sin(\beta) \tag{12}$$

with ω that corresponds to the angular velocity of the wheel of radius r, while v is the velocity of the vehicle and β is the slip angle.
The scalar function $C_{0i}(v_r)$ (with i = x, y) is peculiar of the LuGre model and is given by:

$$C_{0i}(v_r) = \frac{\lambda(v_r)\sigma_{0i}}{\mu_{ki}^2} \tag{13}$$

with

$$\lambda(v_r) = \frac{||M_k^2 v_r||}{g(v_r)} \tag{14}$$

In Eq. 14 we recognize the the matrix of the kinetic friction coefficients $M_k = \begin{bmatrix} \mu_{kx} & 0 \\ 0 & \mu_{ky} \end{bmatrix} > 0$ for the motion along the x and the y directions, respectively; note also that each parameter μ_{ki} in Eq. (13) corresponds to one element on the main diagonal of matrix M_k. We find also the function $g(v_r)$, given by:

$$g(v_r) = \frac{\left\|M_k^2 v_r\right\|}{\|M_k v_r\|} + \left(\frac{\left\|M_s^2 v_r\right\|}{\|M_s v_r\|} - \frac{\left\|M_k^2 v_r\right\|}{\|M_k v_r\|}\right) e^{-\left(\frac{\|v_r\|}{v_s}\right)^\gamma} \tag{15}$$

with $M_s = \begin{bmatrix} \mu_{sx} & 0 \\ 0 & \mu_{sy} \end{bmatrix} > 0$ that is the matrix of static friction coefficients.
To evaluate the constants κ_i^{ss} and ν^{ss}, we do the hypothesis that the steady-state solution of the lumped model is the same with the steady-state solution of the distributed one. The complete expression of these parameters is given from:

$$\kappa_i^{ss} = \frac{1}{|\omega r|}\left(\frac{v_{ri}}{\bar{z}_i^{ss}} - C_{0i}(v_r)\right) \tag{16}$$

$$\nu^{ss} = \frac{1}{|\omega r|}\left(\frac{1}{\hat{z}_y^{ss}}\left(\frac{G v_{ry}}{F_n L} + \frac{|\omega r|\bar{z}_y^{ss}}{L}\right) - C_{0y}\right) \tag{17}$$

with $\bar{z}_i^{ss}$ and $\hat{z}_y^{ss}$, that are the steady-states of the system; the explicit expression for these parameters is given in the appendix of [5].
The auto-aligning torque can be written in terms of the mean states $\bar{z}_y(t)$ and $\hat{z}_y(t)$ as follows:

$$\begin{aligned} M_{self-alig} = F_n L\Big[&\sigma_{0y}\left(\frac{1}{2}\bar{z}_y(t) - \hat{z}_y(t)\right) \\ &+ \sigma_{1y}\left(\frac{1}{2}\dot{\bar{z}}_y(t) - \dot{\hat{z}}_y(t)\right) \\ &+ \sigma_{2y}\left(\frac{1}{2}v_{ry} - \frac{G}{F_n L}\right)\Big] \end{aligned} \tag{18}$$

To calculate the sticking torque we introduce the last equation

$$\dot{z}_z = \dot{\phi} - \frac{\sigma_{0z}|\dot{\phi}|}{g_z(\dot{\phi})} z_z(t) \tag{19}$$

TABLE II

CONSTANT PARAMETERS OF THE LUGRE MODEL

Symbol	Value	Description
r	wheel radius	$0.38\ [m]$
v	vehicle speed	range from 0 to 30 $[km/h]$
ω	angular velocity of the wheel	$\omega = \frac{v}{r}\ [rad/s]$
μ_{kx}	kinetic friction coeff. x-axis	0.75
μ_{ky}	kinetic friction coeff. y-axis	0.75
μ_{kz}	kinetic friction coeff. z-axis	0.76
μ_{sx}	static friction coeff. x-axis	1.35
μ_{sy}	static friction coeff. y-axis	1.40
μ_{sz}	static friction coeff. z-axis	0.91
v_s	Stribeck relative velocity	$3.96\ [m/s]$
$\dot{\phi}_s$	Stribeck relative velocity	$74\ [rad/s]$
γ	steady state constant	1
σ_{0y}	normalized rubber stiffness	$6000\ [N/m]$
σ_{1y}	normalized rubber damping	$0.3568\ [N/m/s]$
σ_{2y}	normalized viscous relative damping	$0.0001\ [N/m/s]$
L	patch length	$0.15\ [m]$
ζ_L	left patch length	$0.0030\ [m]$
ζ_R	right patch length	$0.1155\ [m]$
F_{max}	max value of normal load distribution	$1900\ [N]$
F_n	normal value of normal load distribution	$249.37\ [N]$
α_1	coeff. for Self-Align. torque	$63000\ N/m$
α_2	coeff. for Self-Align. torque	$-55000\ N/m$
β_2	coeff. for Self-Align. torque	$8260\ N$
σ_{0z}	coeff. for Stick. torque	20
σ_{1z}	coeff. for Stick. torque	0.0023
σ_{2z}	coeff. for Stick. torque	0.0001
G	load distribution function	$16.83\ Nm^2$
κ^{ss}	function used to approx. steady behavior	11.9
ν^{ss}	function used to approx. steady behavior	-0.8

where the angular velocity of the wheel rim is $\dot{\phi} = \dot{\theta}_s/N_1$, and and the function

$$g_z\left(\dot{\phi}\right) = \mu_{kz} + (\mu_{sz} - \mu_{kz})\, e^{-\left(\frac{\dot{\phi}}{\dot{\phi}_s}\right)^2} \tag{20}$$

where μ_{kz} and μ_{sz} are, respectively, the kinetic and static friction coefficients across the z-axis, while $\dot{\phi}_s$ is the Stribeck velocity.
The sticking torque can be evaluated as follows:

$$M_{sticking} = -LF_n(\sigma_{0z} z_z(t) + \sigma_{1z}\dot{z}_z(t) + \sigma_{2z}\dot{\phi}) \tag{21}$$

Hence, the total torque generated by the contact of the tyres and the road is:

$$\tau_a = M_{self-alig} + M_{sticking} \tag{22}$$

The parameters used in this model are reported in Table II.

B. Friction model improvements

One possible improvement of the previous model concerns the the dependence of the sticking torque to the vehicle velocity, v. In fact, it can be proved experimentally that, as the speed of the vehicle grows, the self-alignment torque dominates over the sticking torque, and inversely. The previous model in its actual form, does not respect this observation. It is then necessary to weight the sticking torque as a function the velocity of the vehicle. Thus, a possible modification along these observations is

$$M_{sticking} = -LF_n(\sigma_{0z} z_z + \sigma_{1z}\dot{z}_z + \sigma_{2z}\dot{\phi})e^{-|v|/v_k} \tag{23}$$

where v_k is a positive constant.

C. Dependency on the vehicle's speed

It is also important to check if the results follow the expected logic when we vary the vehicle's speed. In order to do this, several simulations were carried out for velocities going from 0 to 30 km/h and over a range time of several seconds, in order to see the effects at steady-state. The choice of this speed range is due to the fact that an EPSs operate in this range.

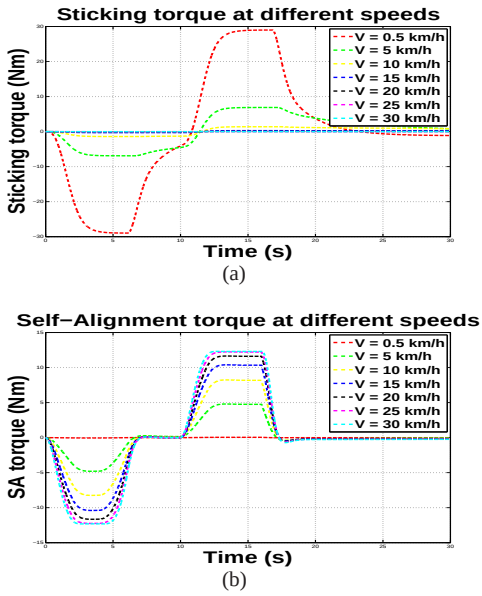

Fig. 6. (a) Sticking torque for different driving speeds (b) Self-Alignment torque for different driving speeds

The results obtained from those simulations are shown by Fig. 6. Fig. 6(a) shows the different curves obtained for the sticking torque for different driving speeds, while Fig. 6(b) shows the different curves obtained for the self-alignment torque. Results are as expected: the sticking torque decreases exponentially as the velocity increases, so as the contribution of the self-alignment is more important as the speed increases.

IV. EXOGENOUS TORQUES ESTIMATION

The purpose of this section is to develop an estimator that includes estimation of the exogenous torques that appear in the system. Both τ_v and τ_a are not sensed *a priori*. By constructing an observer for the "extended" systems the implementation of the previous controller can be done under the relaxing hypothesis on the known and sensed information. Another interesting issues, which is a side effect, is the observer not only provide the control states estimates but also provide an estimate of the driver delivered torque, and the contact tire/road friction forces.

A. Extended state-space representation

Let consider that both exogenous torques are slowly time-varying: $\dot{\tau}_a = \dot{\tau}_v \approx 0$. The extended state-space representation with z now defined as,

$$\tilde{z} = \left(\dot{\theta}_v, \dot{\theta}_s, \theta_v - \theta_s, \tau_v, \tau_a\right)^T \tag{24}$$

in which both exogenous torques are added as state variables, is give by

$$\dot{\tilde{z}} = \tilde{A}_e\tilde{z} + \tilde{B}_e u \tag{25}$$

The state matrices for this system are shown below:

$$\tilde{A}_e = \begin{pmatrix} A & G \\ \mathbb{O}_{2\times 3} & \mathbb{O}_{2\times 2} \end{pmatrix}; \quad \tilde{B}_e = \begin{pmatrix} B \\ 0 \\ 0 \end{pmatrix}; \quad C_e = \begin{pmatrix} C & 0 & 0 \end{pmatrix} \tag{26}$$

If only the motor velocity is used as a available output, then the observability matrix for this new extended system has rank 4 in spite of dealing with a system of dimension 5.

B. Using the torsion force as a additional output

Although it has been so far considered that the only measurable variable was the angular velocity of the assistance motor, it is as well possible to measure a second signal: the torsion force,

$$y_2 = k(\theta_v - \theta_s) = kx_3.$$

In this case, the output matrix C_e of the extended system becomes,

$$\tilde{C}_e = \begin{pmatrix} 0 & 1 & 0 & 0 & 0 \\ 0 & 0 & k & 0 & 0 \end{pmatrix}.$$

Computing the new resulting observability matrix, it can be easily check that it has now full rank. The system is then observable and it is concluded that both exogenous torques can be correctly estimated. The method used to design the observer's gain is analog to the one used in section II-B, i.e. the poles of the observer's dynamic (matrix $\tilde{A}_e - L_e\tilde{C}_e$) should be fast enough compared to those resulting from the linear controller.

The performances of the observer have been tested in simulations. The results obtained for the estimation of τ_v and τ_a are shown in Fig. 7(a) and Fig. 7(b). The maximum value reached by the observation error can be reduced at the price of increasing the observer gain. Measurement noise will limit at certain point the maximum possible value of the observer gain.

V. Conclusions

This paper presented simulation results of a detailed model of an EPS system including a dynamic model that reproduces the physical phenomena involved in driving. From an adequate mechanical model of the steering column, the natural oscillations that exist were eliminated by using a suited optimal linear control design. Furthermore,a highly reliable modified dynamic friction model has been devised from previous author works. This model will allow to carry out trustworthy simulations that will be used to evaluate the different typologies of the potential drives for the new generation of EPSs.

Finally, a satisfactory observer for the internal state variables needed for control, but also for the exogenous torque estimation due to the driver and tire/road friction contact was proposed. This observer was evaluated via simulation on the context of closed-loop showing good results and good estimation characteristics.

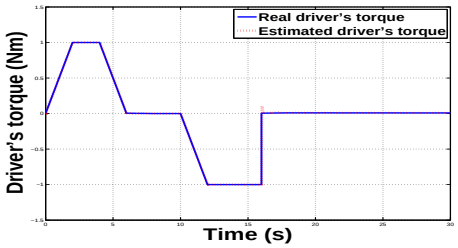

(a)

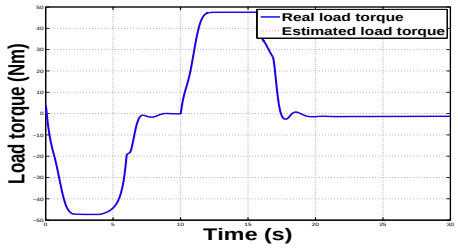

(b)

Fig. 7. (a) Real driver's torque (solid) vs. estimated driver's torque (dotted). (b) Real load torque (solid) vs. estimated load torque (dotted).

VI. Acknowledgements

This work was partially funded by the project VOLHAND ANR-09-VTT-14.

References

[1] Parmar, M.; Hung, J.Y.; , "A sensorless optimal control system for an automotive electric power assist steering system," Industrial Electronics, IEEE Transactions on , vol.51, no.2, pp. 290- 298, April 2004

[2] Morita, Y.; Torii, K.; Tsuchida, N.; Iwasaki, M.; Ukai, H.; Matsui, N.; Hayashi, T.; Ido, N.; Ishikawa, H.; , "Improvement of steering feel of Electric Power Steering system with Variable Gear Transmission System using decoupling control," Advanced Motion Control, 2008. AMC '08. 10th IEEE International Workshop on , vol., no., pp.417-422, 26-28 March 2008

[3] C. Canudas de Wit, S. Guégan, and A. Richard *"Control design for an electro power steering system: part I The reference model"*, ECC'2001, European Control Conference, Porto(Portugal), septembre 2001 (invited)

[4] C. Canudas de Wit, S. Guégan, and A. Richard *"Control design for an electro power steering system: part II The control design"*, ECC'2001, European Control Conference, Porto(Portugal), septembre 2001 (invited)

[5] E. Velenis, P. Tsiotras, C. Canudas de Wit and M. Sorine *"Dynamic Tire Friction Models for Combined Longitudinal and Lateral Vehicle Motion"*, Vehicle System Dynamics, Volume 43, Issue 1 January 2005

[6] C. Canudas de Wit, P. Tsiotras, E. Velenis, M. Basset, and G. Gissinger, *"Dynamic friction models for road/tire longitudinal interaction"*, Vehicle System Dynamics, vol. 39, no. 3, pp. 189 to 226, 2003